







Article

An XAI Framework for Predicting Wind Turbine Power under Rainy Conditions Developed Using CFD Simulations

Ijaz Fazil Syed Ahmed Kabir ^{1,†} , Mohan Kumar Gajendran ^{2,†} , Prajna Manggala Putra Taslim ¹ ,
Sethu Raman Boopathy ¹ , Eddie Yin-Kwee Ng ^{1,*}  and Amirfarhang Mehdizadeh ² 

¹ School of Mechanical and Aerospace Engineering, Nanyang Technological University, 50 Nanyang Avenue, Block N3, Singapore 639798, Singapore; ijaz0001@e.ntu.edu.sg (I.F.S.A.K.); ptaslim001@e.ntu.edu.sg (P.M.P.T.); sethu1@e.ntu.edu.sg (S.R.B.)

² School of Science and Engineering, University of Missouri-Kansas City, Kansas City, MO 64110, USA; mgz53@mail.umkc.edu (M.K.G.); mehdizadeha@umkc.edu (A.M.)

* Correspondence: mykng@ntu.edu.sg

[†] These authors contributed equally to this work.

Abstract: Renewable energy sources are essential to address climate change, fossil fuel depletion, and stringent environmental regulations in the subsequent decades. Horizontal-axis wind turbines (HAWTs) are particularly suited to meet this demand. However, their efficiency is affected by environmental factors because they operate in open areas. Adverse weather conditions like rain reduce their aerodynamic performance. This study investigates wind turbine power prediction under rainy conditions by integrating Blade Element Momentum (BEM) theory with explainable artificial intelligence (XAI). The S809 airfoil's aerodynamic characteristics, used in NREL wind turbines, were analyzed using ANSYS FLUENT and symbolic regression under varying rain intensities. Simulations at a Reynolds number (Re) of 1×10^6 were performed using the Discrete Phase Model (DPM) and $k-\omega$ SST turbulence model, with liquid water content (LWC) values of 0 (dry), 10, 25, and 39 g/m³. The lift and drag coefficients were calculated at various angles of attack for all the conditions. The results indicated that rain led to reduced lift and increased drag. The innovative aspect of this research is the development of machine learning models predicting changes in the airfoil coefficients under rain with an R^2 value of 0.97. The proposed XAI framework models rain effects at a lower computational time, enabling efficient wind farm performance assessment in rainy conditions compared to conventional CFD simulations. It was found that a heavy rain LWC of 39 g/m³ could reduce power output by 5.7% to 7%. These findings highlight the impact of rain on aerodynamic performance and the importance of advanced predictive models for optimizing renewable energy generation.

Keywords: wind turbines; rainy weather impact; blade element momentum theory; computational fluid dynamics; S809 airfoil analysis; symbolic regression; explainable AI; aerodynamic optimization; $k-\omega$ SST model; discrete phase modeling; energy efficiency; predictive analytics



Citation: Syed Ahmed Kabir, I.F.; Gajendran, M.K.; Taslim, P.M.P.; Boopathy, S.R.; Ng, E.Y.-K.; Mehdizadeh, A. An XAI Framework for Predicting Wind Turbine Power under Rainy Conditions Developed Using CFD Simulations. *Atmosphere* **2024**, *15*, 929. <https://doi.org/10.3390/atmos15080929>

Academic Editor: Leonardo Primavera

Received: 19 June 2024

Revised: 19 July 2024

Accepted: 29 July 2024

Published: 3 August 2024



Copyright: © 2024 by the authors. Licensee MDPI, Basel, Switzerland. This article is an open access article distributed under the terms and conditions of the Creative Commons Attribution (CC BY) license (<https://creativecommons.org/licenses/by/4.0/>).

1. Introduction

Wind energy continues to play a crucial role in the global shift toward renewable energy sources, witnessing significant growth in installed capacity and its contribution to global electricity production. Reports from the International Energy Agency (IEA) [1] and the Global Wind Energy Council [2] confirm the upward trend in wind energy adoption, underscoring its importance in meeting carbon reduction targets. This global commitment directly influences national policies and fosters the expansion of wind energy projects worldwide [3].

The performance of wind turbines is significantly influenced by weather conditions, particularly rain, which affects their aerodynamic efficiency. Rainfall impacts the air density and viscosity around the turbine blades, altering their aerodynamic properties [4,5]. This interaction leads to shifts in the laminar–turbulent transition on the blade surfaces [6].

Understanding these hydrodynamic effects is crucial in evaluating how weather conditions affect turbine performance [7].

Research on the impact of rainfall initially focused on the aerodynamic performance of aircraft in such conditions. Over the past few decades, extensive computational fluid dynamics (CFD) and experimental investigations have explored how rainfall affects aircraft airfoils. Notable experimental studies include those by Rhode [8], Hansman and Barsotti [9], Hansman and Craig [10], Marchman et al. [11], and Bezos [12]. Prominent CFD studies include those by Valentine and Decker [13], Thomson and Marrochello [14], Tan et al. [15], Wan and Wu [16], and Zhang and Cao [17]. These studies commonly used NACA airfoils, particularly the NACA 64-210 and NACA 0012, revealing that rain decreases the lift coefficient and increases the drag coefficient. Below is a concise review of the investigation of rainfall on airfoils used in wind turbines.

In 2012, Douvi and Margaris [18] applied a two-phase flow approach in CFD to analyze the aerodynamic characteristics of a NACA 0012 airfoil under dry and simulated heavy rain conditions with a liquid water content (LWC) of 30 g/m^3 . Their analysis at higher Reynolds numbers (1×10^6 and 3×10^6) showed that heavy rain worsens aerodynamic performance, reducing the lift coefficient and increasing the drag coefficient. They also demonstrated a decline in the power coefficient of a two-bladed horizontal-axis wind turbine in severe rain, with a percentage shift in the power coefficient ranging from 2% to 7% depending on the blade angle of attack. However, the methods used to calculate the power coefficient, such as the Blade Element Momentum (BEM) approach, were not specified.

In 2012, Cai et al. [19] conducted a multiphase CFD simulation using the coupled Lagrangian–Eulerian technique to evaluate the S809 airfoil’s performance in rainy weather, finding that intense precipitation significantly reduces efficiency.

In 2013, Douvi et al. [20,21] investigated various rainfall rates’ impact on the NACA 0012 airfoil’s aerodynamic properties using both computational and experimental methods at a low Reynolds number (1×10^5). Their research revealed that increased LWC led to more significant aerodynamic deterioration, especially up to the stall angle, and that stall onset was delayed at all rainfall rates.

In 2016, Cohan and Arastoopour [22] evaluated the S809 wind turbine airfoil’s performance under different precipitation rates using coupled Discrete Phase Model (DPM) and Volume Of Fluid (VOF) 2D CFD analyses. They observed that the airfoil’s performance is extremely sensitive to the rainfall rate during periods of minimal precipitation. However, subsequent increases in rainfall do not significantly affect the performance of the airfoil once the rate of precipitation is adequate to generate a water film on its surface. They discovered intriguing results indicating that at higher rainfall rates, the lift coefficient is greater than in the absence of rain, but this is accompanied by an unfavorable increase in the drag coefficient, whereas previous research suggested that rain only causes a decrease in the lift coefficient.

In 2017, Wu et al. [4] conducted a study on a two-way coupled Eulerian–Lagrangian multiphase technique to examine the behavior of the NACA 0015, an extensively used airfoil in vertical-axis wind turbines (VAWTs), in rainy circumstances. They found that rain significantly impairs VAWT performance, with higher LWC and larger raindrop diameters exacerbating performance deterioration.

In 2021, Douvi et al. [23] studied the impact of rainfall on the aerodynamic performance of a horizontal-axis wind turbine (HAWT) with a NACA 4418 airfoil using ANSYS FLUENT using Multiple Reference Frame (MRF) analysis. They observed substantial decreases in aerodynamic efficiency in wet conditions compared to dry, with reductions of 11.84%, 16.87%, and 23.9% for LWCs of 10 g/m^3 , 30 g/m^3 , and 60 g/m^3 , respectively. Increasing the raindrop diameter while maintaining a constant LWC further decreased the power coefficient.

In 2022, Gahlot et al. [24] conducted RANS simulations on the S809 airfoil, showing a 30% to 40% decrease in power generation due to rainfall across various wind speeds. Wu et al. [25] used the Eulerian multiphase single-rotating frame collision theory method (ESCM-

WAR) hybrid approach to study 5 MW floating wind turbines in wind–rain conditions, finding that the thrust and torque from the rain load increased with the rainfall intensity.

In 2023, Hu et al. [26] experimented with how rainfall affected wind turbine blade aerodynamic performance under different test settings. The experiment used a common wind turbine airfoil/blade model at Iowa State University’s Icing Research Tunnel. They measured the lift and drag forces on the airfoil/blade model as a function of the inflowing airflow speed and rainfall rate. They also employed a high-resolution digital PIV system to assess the raindrop impingement-induced airflow characteristics over the airfoil/blade model and their correlations with rainfall-induced aerodynamic deterioration under different test settings.

Recently, in 2024, Letzgus and Müller [27] developed an explainable AI framework for robust and transparent data-driven wind turbine power curve models. However, this work focused on determining the power from wind turbine operational data and does not address the effects of rain. In contrast, our work focuses on the effects of rain and is suitable for the design phase. The present state of the art in previous studies predominantly shows that rain reduces the lift coefficient and increases the drag coefficient of airfoils. However, there is a lack of specific models quantifying these aerodynamic changes. Addressing this research gap, our innovative contribution lies in developing explainable AI (XAI) models specifically for the S809 airfoil, commonly used in NREL wind turbines. By generating data for various rainy conditions, we create a symbolic regression model that predicts the effects of rain on the airfoil’s aerodynamic performance. The uniqueness of this work is the application of a machine learning model, which we integrate with Blade Element Momentum (BEM) theory to predict the power. This integration allows for the prediction of wind turbine power under varying rain conditions at a significantly reduced computational cost. The objectives of this study are to advance the current understanding of rain effects on wind turbines and provide a practical, efficient method for predicting wind turbine performance in rain conditions using machine learning, thus filling a critical gap in the literature.

This study combines computational fluid dynamics (CFD) and explainable artificial intelligence (XAI) techniques like symbolic regression to create a comprehensive predictive framework. CFD provides detailed simulations of the rain impact on airflow and aerodynamics prediction. Using the insights gained from the CFD and symbolic regression models, Blade Element Momentum (BEM) theory offers predictions on the aerodynamic performance of wind turbine blades under varying rain conditions. By leveraging these advanced modeling techniques, this research enhances the predictive accuracy of turbine performance under rainy conditions, optimizes energy output, and extends the lifespan of turbine components, contributing to the sustainability and resilience of wind energy systems.

To ensure thorough comprehension of our investigation, we have structured this paper into the following subsections: Section 2.1 describes the two-phase CFD modeling approach used to simulate the impact of rain on the airfoil. Section 2.2 details the machine learning model employed for symbolic regression. Section 2.3 provides an overview of the Blade Element Momentum (BEM) theory. Section 3 discusses the findings from our CFD analyses and XAI models, along with their BEM implications. This comprehensive approach ensures accurate predictions of wind turbine performance in rainy conditions.

2. Methodology

The S809 airfoil is a widely utilized airfoil in the design of wind turbine blades, especially those developed by the National Renewable Energy Laboratory (NREL). Its performance characteristics under various conditions are thoroughly researched, making it an ideal candidate for studies focused on wind energy. The rationale for choosing the S809 airfoil in this study is twofold. Firstly, its established use in NREL wind turbines provides a reliable foundation for our research, ensuring that our findings are applicable to real-world scenarios. Secondly, the authors have a history of employing the NREL Phase VI wind turbine in their previous work [28,29], which utilizes the S809 airfoil. This continuity allows us to build on prior research, enhancing the relevance of our current study on the

aerodynamic impacts of rain on wind turbine performance. The methodology for this paper involves several key steps, starting with data generation through computational fluid dynamics (CFD) simulations using the S809 airfoil.

CFD with the Reynolds-Averaged Navier–Stokes (RANS) and Discrete Phase Model (DPM) is utilized to model the effects of rain on the aerodynamic performance of the airfoil, specifically focusing on the lift coefficient (C_L) and drag coefficient (C_D).

The generated data are then employed to train a symbolic regression-based explainable artificial intelligence (XAI) model. The results from the XAI model are subsequently input into the Blade Element Momentum (BEM) theory to calculate the forces, which are further used to determine the power output of the wind turbine.

This entire process is illustrated in the flow chart shown in Figure 1. Each of these steps is detailed in the following subsections. Figure 2 provides a more detailed explanation of the rain model development part.

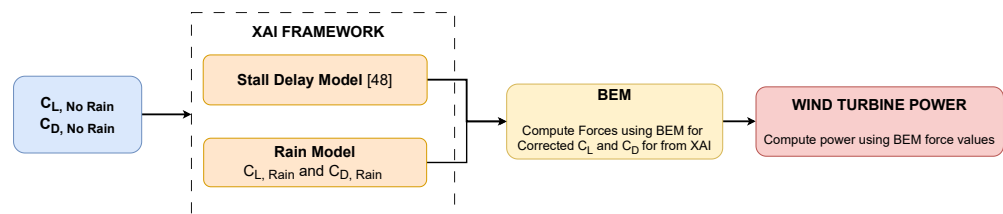


Figure 1. Overall flowchart describing development of XAI-based framework for prediction of power during rainy conditions.

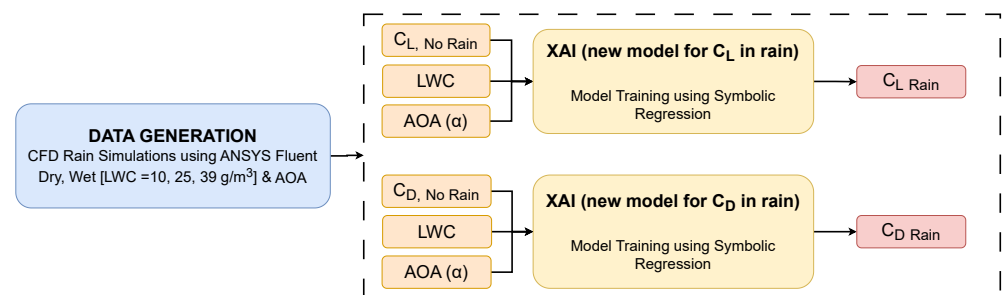


Figure 2. Flowchart describing XAI-based framework for rain model development.

2.1. Data Generation Using CFD Simulations

2.1.1. Rain Modeling

Rain modeling involves characterizing raindrop sizes, their distribution, and their interactions with the wind. Accurate models are essential for simulating and understanding the dynamics of rainfall. Two critical parameters in rain modeling are liquid water content (LWC) and terminal velocity (U_T), which significantly influence the behavior and impact of rainfall in computational simulations.

Liquid Water Content (LWC)

The intensity of rainfall is a critical factor in the CFD modeling of precipitation. Liquid water content (LWC) is a significant parameter often used to quantify the intensity of rainfall [30]. LWC refers to the mass of liquid water present per unit volume of air, often measured in grams per cubic meter (g/m^3) [30]. Previous studies have utilized various LWC values, including 3, 8.7, 10, 14.6, 16, 20.548, 23, 25, 30, 37.745, 39, 41.096, 44, 46, 60, 75.491, and $80 \text{ g}/\text{m}^3$ [3,4,9,10,12,13,16,18,20,21,24,31–37]. For this study, we selected three commonly used and evenly spaced levels of LWC: 10, 25, and $39 \text{ g}/\text{m}^3$.

Terminal Velocity (U_T)

The behavior of a raindrop in the atmosphere is not characterized by free fall; its velocity does not necessarily increase with distance or time of descent. As a raindrop descends,

it is subjected to aerodynamic drag and buoyancy forces in addition to gravity [38]. The resistance of the air increases as the speed of the raindrop increases until it reaches the utmost velocity, which is known as the terminal velocity, at which point the gravitational force is equivalent to the resultant force of the drag and the buoyancy. Afterward, the raindrop will descend at a consistent terminal velocity [30] prior to making impact with the airfoil surface [37]. Markowitz [39] developed the widely used formula for terminal velocity shown in Equation (1), which depends on the raindrop size.

$$U_T = 9.58 \left(1 - \exp \left[- \left(\frac{D_p}{1.77} \right)^{1.147} \right] \right) \quad (1)$$

where D_p represents the diameter of the raindrop in mm.

The raindrop diameters reported in various studies [3,4,9,10,13,16,18–22,24,25,32–34,36] range from 0 to 6 mm, with approximately 1 mm being the most frequently used. Consequently, the size of the raindrop used in this study was 1 mm.

2.1.2. Computational Fluid Dynamics (CFD) Setup

Numerical Modeling

The modeling of the impact of rain on the airfoil is achieved using a two-phase flow method that relies on the Eulerian–Lagrangian technique. The Eulerian–Lagrangian technique solves the conservation equations for the continuous phase and integrates the equations of motion for the discrete phase. This method is known as the Discrete Phase Model (DPM) approach [40]. This study treats air as a continuous phase, whereas raindrops are treated as a discrete phase. The air, considered as a continuous fluid phase, is analyzed by solving the Reynolds-Averaged Navier–Stokes (RANS) transport equations. The raindrops as a discrete phase is resolved by tracking the individual droplets within the computed airflow field. In this technique, the discrete phase has the ability to exchange momentum, mass, and energy with the continuous phase. In this investigation, the subsequent assumptions are implemented: the flow is regarded as incompressible; raindrops are presumed to be non-evaporating, non-interacting, and maintain a spherical shape before deformation; and the trajectories of the rain droplets are estimated at specified intervals throughout the fluid phase simulation. ANSYS FLUENT [40] has the ability to forecast the trajectory of raindrops by estimating the force balance on the rain particle using a Lagrangian reference frame. Further information on the Discrete Phase Model (DPM) can be obtained in the literature [4,18–22,32–37,40–43].

Model Description and Boundary Conditions

The simulations were performed on a computational domain in two dimensions. The inlet had a uniform velocity of 14.2070 m/s, which corresponds to a chord length of 1 m and a Reynolds number (Re) of 1×10^6 . The airfoil surface was subjected to the no-slip condition, and the outlet was designated as a fixed pressure outlet. External effects on the flow field around the airfoil were prevented by the computational domain's ample size. An 8 m chord injection line was chosen to inject rain particulates into the airfoil, and it was positioned 2 chord lengths upstream of the leading edge of the airfoil.

Equation (1) was used to calculate the terminal velocity, which was 3.9 m/s, because the diameter of the raindrop was 1 mm. In our particular case, the volume flow rate was 113.656 m³/s, as we estimated an injection area of 8×1 m (unit width) and a free stream velocity of 14.2070 m/s, as illustrated in Figure 3. Based on the computed volume flow rate above, the mass flow rates of the rain were 1.14, 2.84, and 4.43 kg/s for the rain conditions of LWC 10, 25, and 39 g/m³, respectively. The mass flow rate for each injection point was 0.00189, 0.0047, and 0.0074 kg/s for LWC 10, 25, and 39 g/m³, respectively, as we considered 600 injection points. The k – ω SST turbulence model was implemented in ANSYS FLUENT 2023. Calculations were conducted for angles of attack (AOA) that ranged from 0 to 12.23 degrees.

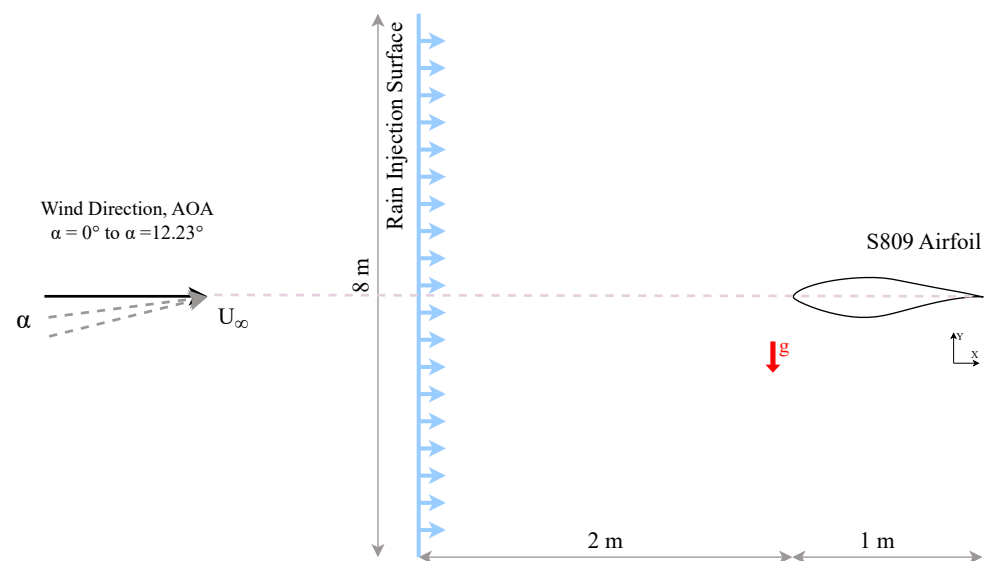


Figure 3. Sketch illustrating the rain modeling method used in this study, describing the injection surface placement in front of the airfoil.

Computational Grids and Grid Independence Study

The computational domain was discretized using structured C-type grids. Four distinct grids were used to calculate the lift coefficients for the purpose of conducting grid independence research. Four grids were produced for the S809 airfoil, each with a different number of cells: approximately 250,000, 500,000, 750,000, and 1,000,000. Figure 4 shows the comparison of the lift coefficients at an angle of attack of 8.2° for four distinct grids, along with the corresponding experimental value under dry conditions. Table 1 shows the average Y^+ values around the airfoil for the four distinct grids that were taken into account. The C_L value for a grid size of 1 million closely matches the experimental data and the Y^+ value is below 2. Furthermore, ANSYS FLUENT is only able to utilize grids with a maximum of 1,048,576 cells due to the limitations of the student license. In our particular case, a grid with one million cells yields satisfactory results, and due to the limitations, this mesh was finished in preparation for further investigation.

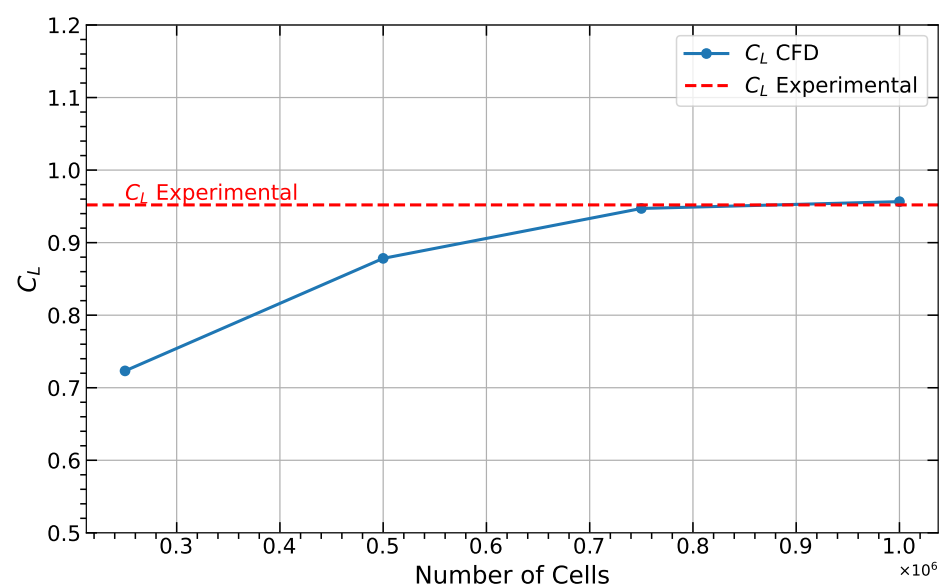


Figure 4. The number of cells vs. the lift coefficient (C_L). The red dotted line indicates the experimental values from the NREL Report [44].

Table 1. Mesh independent study using $k-\omega$ SST turbulence model.

Number of Cells	Velocity (m/s)	AoA	Ux (m/s)	Uy (m/s)	C_L	AvgY ⁺
250,000	14.2070	8.2000	14.0618	2.0263	0.7232	123.776
500,000	14.2070	8.2000	14.0618	2.0263	0.8783	38.3781
750,000	14.2070	8.2000	14.0618	2.0263	0.9471	16.9811
1,000,000	14.2070	8.2000	14.0618	2.0263	0.9565	1.99931
Experiment [44]					0.952	

2.2. Symbolic Regression (XAI) Model

Symbolic regression is a versatile technique used to approximate mathematical functions [45]. It involves systematically modifying operators within a set of explicit formulae to explore the mathematical space and identify the most appropriate metamodel. These formulae can be represented in a tree structure, and combinatorial optimization techniques are employed to find the optimal tree. Symbolic regression's strengths lie in its interpretability and its ability to uncover underlying physical relationships from data [46]. It offers several benefits over other regression methods, including flexibility in selecting operators, the class of functions, and the expression size.

Simulated annealing (SA), introduced by Kirkpatrick et al. [47], is a popular method used in symbolic regression. This technique starts with a single solution and iteratively explores neighboring solutions, gradually decreasing the probability of accepting worse solutions over time. Simulated annealing's main advantage is its ability to locate a global minimum, along with ease in determining constants and a relatively low computational cost [46].

In simulated annealing-based symbolic regression [48], the algorithm begins with a broad search of the solution space, which becomes more focused as parameters are adjusted during each iteration. The decision to retain the current solution or move to a neighboring one is based on probabilistic criteria that decay over time. While complex functions may fit the data better, they are prone to overfitting and can be difficult to interpret. Therefore, the goal is to find a mathematical expression that is both simple and fits the data well using a multi-objective combinatorial optimization (MOCO) method, such as Pareto-simulated annealing [46].

Pareto-simulated annealing-based symbolic regression as shown in Figure 5 enhances traditional methods by initiating with linear regression for estimating constants and utilizing interval arithmetic to ensure the model's consistency. The process starts with transformation functions represented as binary trees, where nodes signify operators, input parameters, or constants. These functions undergo iterative modifications governed by the Pareto-simulated annealing algorithm, which adjusts the annealing temperature to balance exploration and exploitation effectively. Each iteration involves selecting a random transformation function for modification, ensuring its integrity using interval arithmetic to prevent invalid operations. The coefficients of the transformation functions are recalculated using linear regression, transforming the problem into a linear one and improving computational efficiency. Model quality is assessed using the root mean squared error (RMSE) and validation RMSE to prevent overfitting. Pareto-simulated annealing treats model fit and complexity as separate objectives, generating a Pareto front representing the trade-offs between these two aspects. A novel complexity measure, based on the minimal degree of polynomial necessary for approximation within a predefined error margin, is employed to avoid overfitting and enhance interpretability. Compared to traditional Kriging models and symbolic regression based on genetic programming, Pareto-simulated annealing-based symbolic regression offers several advantages. It efficiently handles constants via linear regression, requires fewer evaluations to converge, and produces more interpretable models. This method demonstrates competitive performance across various test cases, establishing its potential as a robust tool for metamodeling in simulation-based optimization [46]. The detailed algorithm for implementing Pareto-simulated annealing-based symbolic regression is outlined by Stinstra et al. [46] and was executed using the

TuringBot 2.18.1 Python library on an AMD Ryzen™ 9 5900 CPU with 24 threads over approximately 1100 CPU hours.

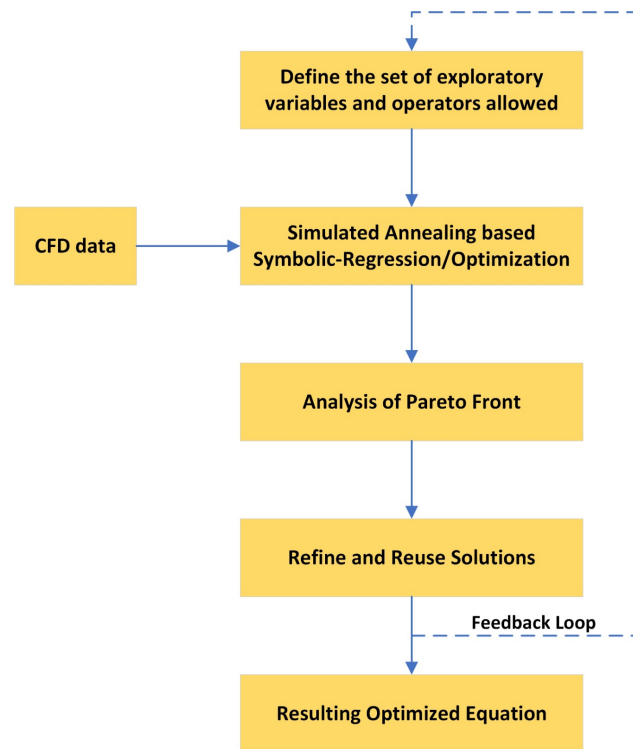


Figure 5. Flow chart explaining symbolic regression procedure.

In this study, we are proposing a new model to capture the effects of rain on aerodynamic performance. The lift coefficient (C_L) and drag coefficient (C_D) under rainy conditions are derived by incorporating rain-induced changes (ΔC_L and ΔC_D). These changes are influenced by the liquid water content (LWC), and the resulting coefficients are calculated as follows:

$$C_{L,\text{rain}} = C_{L,\text{no rain}} + \Delta C_L \quad (2)$$

$$C_{D,\text{rain}} = C_{D,\text{no rain}} + \Delta C_D \quad (3)$$

Here, $C_{L,\text{rain}}$ and $C_{D,\text{rain}}$ represent the lift and drag coefficients under rainy conditions, respectively, while $C_{L,\text{no rain}}$ and $C_{D,\text{no rain}}$ denote the corresponding coefficients in the absence of rain. The terms ΔC_L and ΔC_D capture the differences in the lift and drag coefficients due to rain, which depend on the specific LWC and AOA.

This formulation enables the calculation of aerodynamic coefficients by adding the rain-induced changes to the baseline values obtained under dry conditions. For example, if the LWC is 10 g/m^3 , the changes in the coefficients, ΔC_L and ΔC_D , are evaluated at this LWC and added to $C_{L,\text{no rain}}$ and $C_{D,\text{no rain}}$ to obtain the coefficients under rainy conditions.

Our model provides a systematic approach to understanding and quantifying the impact of rain on aerodynamic performance. It allows for more accurate predictions and adjustments in the design and analysis of airfoils subjected to rainy conditions. The exact model details will be discussed in the Results Section 3.3.

2.3. Integration with Blade Element Momentum (BEM)

The Blade Element Momentum (BEM) hypothesis is extensively used for the purpose of wind turbine design and performance evaluation. This approach combines the principles of momentum theory with blade element theory. Momentum theory is derived from the principles of conserving linear and angular momentums. The rotor is substituted by a permeable or porous disk and partitioned into N concentric elements, with forces being

computed at each element. Blade element theory involves dividing the blade again into N elements and calculating the forces in each element based on the airfoil properties of the lift coefficient (C_L) and drag coefficient (C_D). The process of deriving, implementing, and correcting the BEM technique is well explained in the works of Burton et al. [49], Hansen [50], and Kabir [29].

Multiple software products use the BEM methodology. These are some notable tools: Qblade [51], Aerodyn [52], HAWC2 [53], WTPerf [54], FAST [55], GH Bladed [56], and PHATAS [57]. Furthermore, the present authors in their previous study [29] developed MATLAB code for BEM. A significant drawback of the BEM approach is the occurrence of a 3D phenomenon known as stall delay [28]. To compensate for stall delay, several XAI models have been proposed to be added into the 2D airfoil characteristics [28,29]. The present authors in their previous study [58] developed an XAI model using a machine learning technique, which was proven to be more accurate. Therefore, the authors used a stall delay model based on their previous work [58] to conduct a BEM analysis using MATLAB code [29].

3. Results and Discussion

3.1. Comparison of Dry Condition with Experimental Results

The numerical simulations were performed at a Reynolds number of 1×10^6 across a range of angles of attack from 0° to 17.21° . This study integrates both experimental and predicted C_L and C_D values for the S809 airfoil, sourced from wind tunnel tests conducted at Ohio State University (OSU), Colorado State University (CSU), and the Delft University of Technology (DUT) [28,44]. The experimental data from DUT at the specified Reynolds number were used as a benchmark to validate the numerical simulation results.

In aerodynamic analysis, the airflow around an airfoil causes an increase in velocity on the top (suction) surface, leading to a pressure drop, while the velocity decreases on the bottom (pressure) surface, causing a pressure rise. Additionally, friction between the air and the airfoil surfaces results in further velocity reduction [29]. The resulting force and momentum on the airfoil are due to the pressure differential and skin frictional drag. The net force can be decomposed into two components: lift, which is perpendicular to the airflow direction, and drag, which is parallel [29]. To predict the lift and drag coefficients, the $k-\omega$ SST turbulence model was utilized in the CFD simulations. These predictions were then compared with the experimental data for consistency.

The initial focus of this study was on evaluating the lift and drag coefficients under dry conditions to establish a baseline for later investigations under varying rain conditions. Figure 6 shows the simulation results of the lift coefficient for the S809 airfoil as a function of the angle of attack. The relationship between the lift coefficient and the angle of attack is approximately linear up to 12° . The simulation results correlate well with the experimental data at low to mid-range angles of attack, with minor deviations at higher angles. This pattern is consistent with previous studies of the S809 airfoil at the same Reynolds number [59–61]. These results affirm the reliability of our CFD simulations, supporting their use for further investigations under rainy conditions.

3.2. Impact of Rain Conditions on Airfoil Dynamics

The simulations under rainy conditions were conducted for angles of attack ranging from 0° to 12.23° at liquid water contents (LWCs) of 10, 25, and 39 g/m^3 and a Reynolds number of 1×10^6 . The lift coefficient (C_L) as a function of the angle of attack (AOA) for various rain conditions is shown in Figure 7.

The analysis shows that as the LWC increases, the detrimental effects on aerodynamic performance become more pronounced. At lower LWCs, the reduction in lift is relatively moderate, but as the LWC reaches higher values (25 and 39 g/m^3), the negative impact on the lift becomes substantial. This trend highlights the sensitivity of airfoil performance to rain conditions and underscores the importance of accounting for such factors in aerodynamic designs and assessments.

It is evident from Figure 7 that there is consistent degradation in (C_L) performance with an increase in LWC. The diminution in the lift coefficient varies from 0.85% to 3.74% for the LWC of 10 g/m³, from 1.91% to 8.20% for the LWC of 25 g/m³, and from 2.98% to 12.70% for the LWC of 39 g/m³.

Additionally, Figure 8 clearly demonstrates a steady increase in the (C_D) results as the LWC increases. The increase in the drag coefficient ranges from 1.92% to 6.19% for an LWC of 10 g/m³, from 4.94% to 13.90% for an LWC of 25 g/m³, and from 5.96% to 21.24% for an LWC of 39 g/m³.

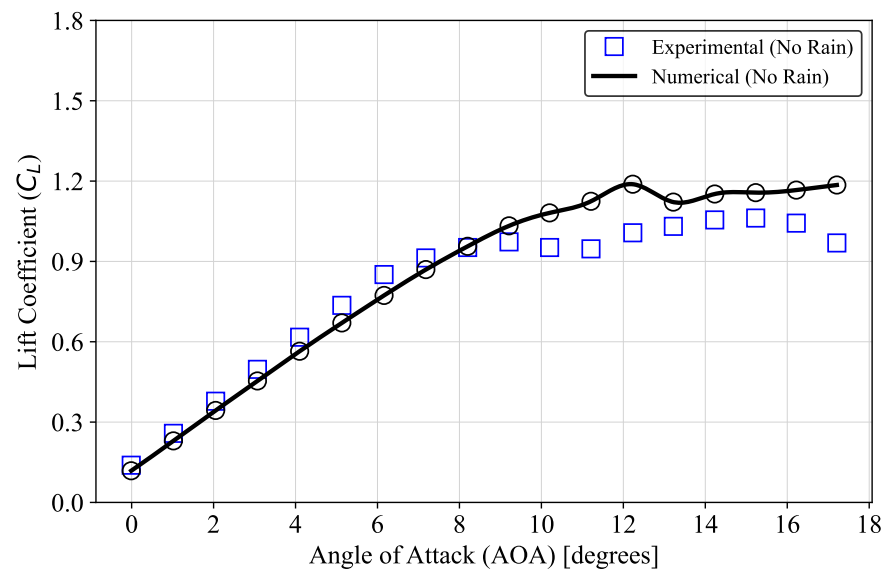


Figure 6. Plot of lift coefficient (C_L) versus angle of attack (AOA) for dry conditions.

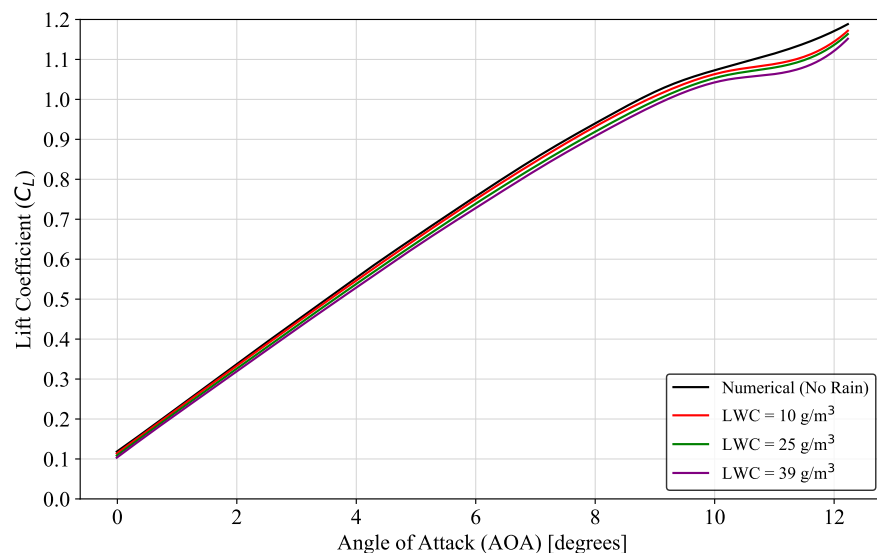


Figure 7. Plot of lift coefficient (C_L) versus angle of attack (AOA) under no rain and various liquid water content (LWC) conditions.

Multiple perspectives are presented in the literature on the factors that contribute to the diminution in aerodynamic performance of airfoils when exposed to rain. This study focuses on the development of corrective models using machine learning that can be used in BEM to address the impact of rain. Below is an overview of the many concepts [24] that have been considered.

- The wavy surface of the water layer on the airfoil may induce this consequence in a way similar to the presence of irregularities or roughness on the airfoil surface.
- The cause for this degradation can also be due to the additional displacement thickness from the water layer and the loss of airflow momentum due to the drag forces exerted by water droplets, which can significantly modify the airfoil's pressure field and eventually alter the force.
- While in computational fluid dynamics (CFD), the walls are assumed to be rigid and erosion is not accounted for, in actuality and experimental assessments, and weathering of the wind turbine blade surface due to rain or water may disrupt the boundary layer and lead to a significant increase in drag.

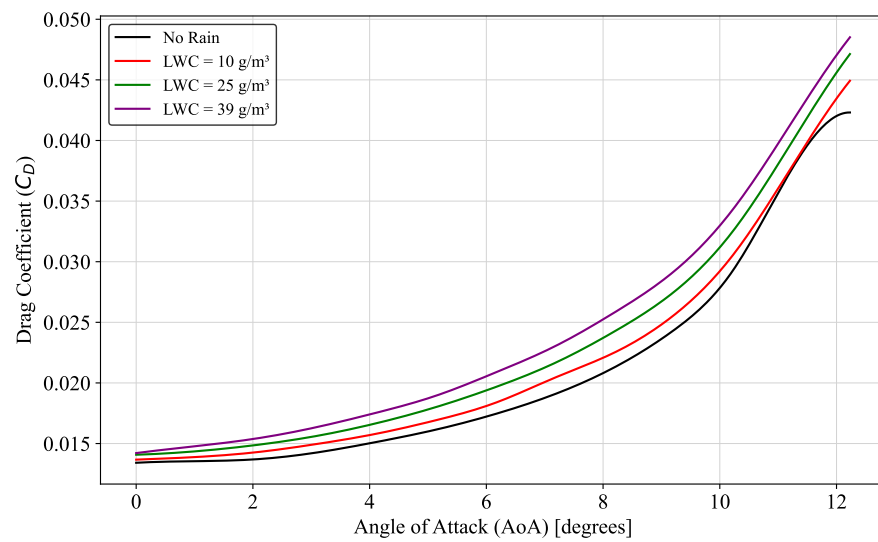


Figure 8. Plot of drag coefficient (C_D) versus angle of attack (AOA) under no rain and various liquid water content (LWC) conditions.

3.3. Proposed XAI Model

In this study, we propose a model to capture the effects of rain on aerodynamic performance. Three non-dimensional exploratory variables, the angle of attack (α), the liquid water content (LWC), and the baseline coefficients ($C_{L,\text{no rain}}$ and $C_{D,\text{no rain}}$), are used to model the rain effect on the lift and drag coefficients. The objective of the symbolic regression algorithm is to determine mathematical expressions for the changes in the lift coefficient (ΔC_L) and drag coefficient (ΔC_D) under rainy conditions. A total of 70 percent of the data were used for training the XAI model. For validation, this study employed a hold-out cross-validation strategy to prevent overfitting: 15 percent of the data were reserved for hyper-parameter tuning and another 15 percent were set aside for testing. The optimized hyper-parameters included the coefficients of the derived functional form.

The expressions for ΔC_L and ΔC_D are given by:

$$\Delta C_L = f(\alpha, \text{LWC}, C_{L,\text{no rain}}) \quad (4)$$

$$\Delta C_D = g(\alpha, \text{LWC}, C_{D,\text{no rain}}) \quad (5)$$

where $f(\alpha, \text{LWC}, C_{L,\text{no rain}})$ and $g(\alpha, \text{LWC}, C_{D,\text{no rain}})$ are functions determined through the symbolic regression process. For the purposes of this study, the dummy equations for these functions are provided as follows:

$$\Delta C_L = C_1 \cdot \text{LWC} \cdot e^{C_2 \cdot \alpha} \cdot \sqrt{C_{L,\text{no rain}}} \quad (6)$$

$$\Delta C_D = C_3 \cdot \text{LWC} \cdot \sqrt{\alpha \cdot C_{D,\text{no rain}}} \quad (7)$$

where $C_1 \approx -0.00083$, $C_2 \approx 0.00278$, and $C_3 \approx 0.00025$ are coefficients determined through the symbolic regression process.

After determining the expressions for ΔC_L and ΔC_D , the lift and drag coefficients under rainy conditions ($C_{L,rain}$ and $C_{D,rain}$) can be computed from the coefficients under no rain ($C_{L,no\ rain}$ and $C_{D,no\ rain}$) using the following equations:

$$C_{L,rain} = C_{L,no\ rain} + \Delta C_L \quad (8)$$

$$C_{D,rain} = C_{D,no\ rain} + \Delta C_D \quad (9)$$

The proposed model captures the impact of rain on aerodynamic performance through three key variables: the angle of attack (α), the liquid water content (LWC), and the baseline coefficients ($C_{L,no\ rain}$ and $C_{D,no\ rain}$). The degradation in lift (ΔC_L) is directly proportional to the LWC, highlighting how rain alters airflow, thereby reducing the lift. Similarly, the drag increase (ΔC_D) is influenced by the LWC and α , demonstrating how rain-induced surface roughness and changes in airflow dynamics lead to higher drag. The selection of α and LWC as input variables ensures the model accurately reflects the physical principles underlying the rain's impact on aerodynamic performance.

The symbolic regression algorithm employed in this study automatically identifies the most relevant parameters and constructs the model using a variety of mathematical operators, such as multiplication, division, exponentiation, and square root. This approach helps avoid overfitting and ensures robustness, allowing the model to generalize well across different conditions. By combining these operators, the algorithm effectively captures the complex relationships between the variables, providing a nuanced and accurate representation of the effects of rain on lift and drag coefficients.

The results from this proposed model, which incorporates the effects of rain into the calculation of ΔC_L and ΔC_D , are then passed to the stall delay correction model developed by the same group [58] to compute the three-dimensional lift coefficient ($C_{L,3D}$) from the two-dimensional lift coefficient ($C_{L,2D}$) with the effects of rain included. Integrating these two models allows for a more comprehensive understanding of both rain effects and stall delay, providing a holistic approach to aerodynamic performance prediction.

This combined model is a crucial component of the proposed explainable AI (XAI) framework, which will subsequently be integrated into the Blade Element Momentum (BEM) method. The enhanced BEM method will utilize these refined aerodynamic coefficients to more accurately compute the power output of wind turbines, accounting for both rain conditions and stall delay effects. This integration ensures that the predictive model captures all relevant physical phenomena, leading to more reliable and robust power calculations.

The results of the proposed model are depicted in Figures 9 and 10. Figure 9 presents the comparison of the lift coefficient ($C_{L,Rain}$) as a function of the angle of attack (AOA) for different liquid water content (LWC) values. Each subplot in this figure represents a different LWC: 10 g/m³, 25 g/m³, and 39 g/m³. Similarly, Figure 10 illustrates the comparison of the drag coefficient ($C_{D,Rain}$) as a function of the AOA for the same LWC values. The proposed model demonstrates a high degree of accuracy with an R^2 value of 0.97 for both coefficients. The formulations for the changes in the lift coefficient and drag coefficient due to rain are given by Equations (4) and (5), respectively.

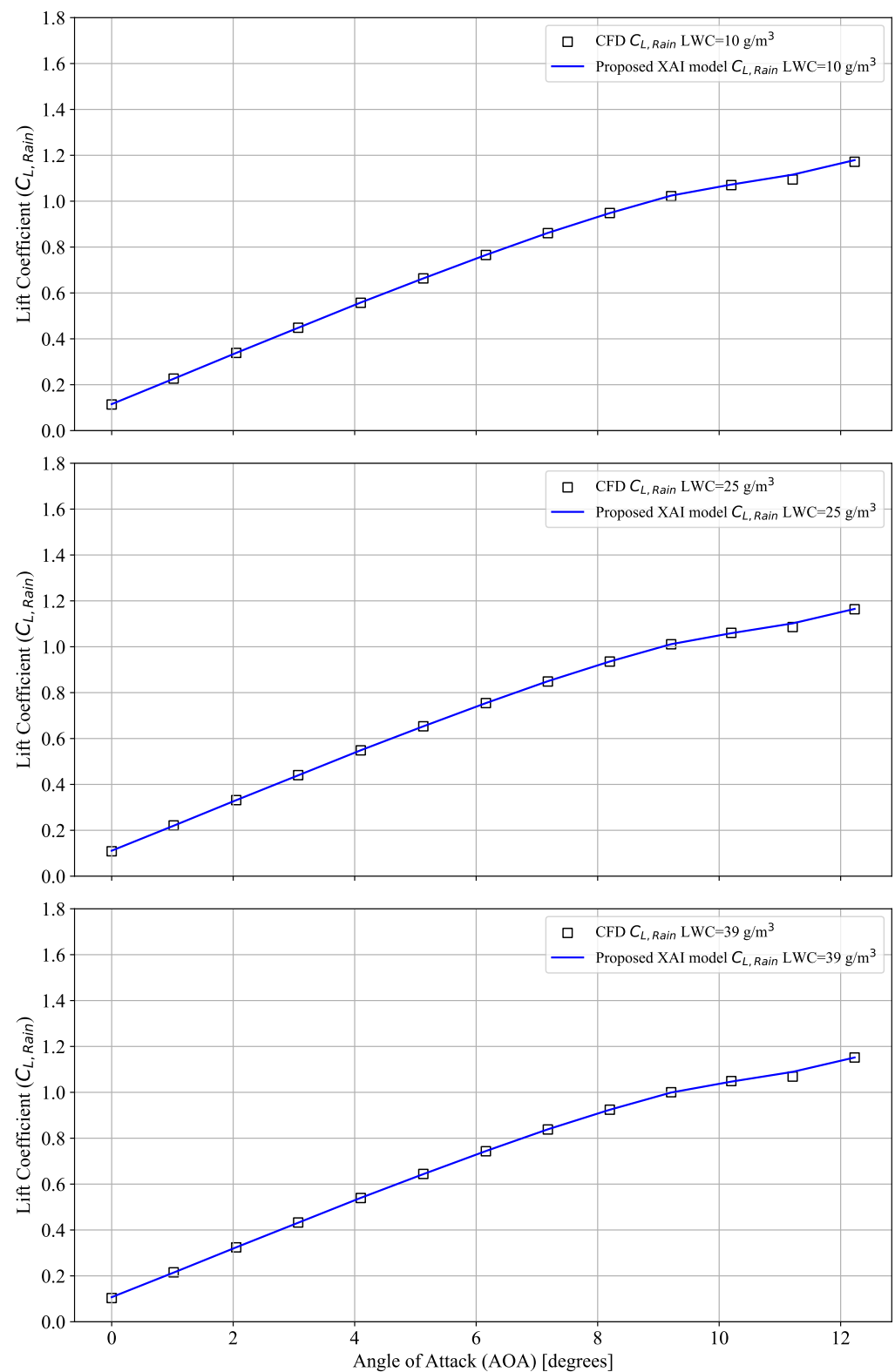


Figure 9. A comparison of the lift coefficient ($C_{L,Rain}$) as a function of the angle of attack (AOA) for different liquid water content (LWC) values. Each subplot represents a different LWC: 10 g/m³, 25 g/m³, and 39 g/m³. The blue line represents the proposed XAI model's $C_{L,Rain}$, while the black hollow squares represent the CFD $C_{L,Rain}$. The model demonstrates a high degree of accuracy with an R^2 value of 0.97.

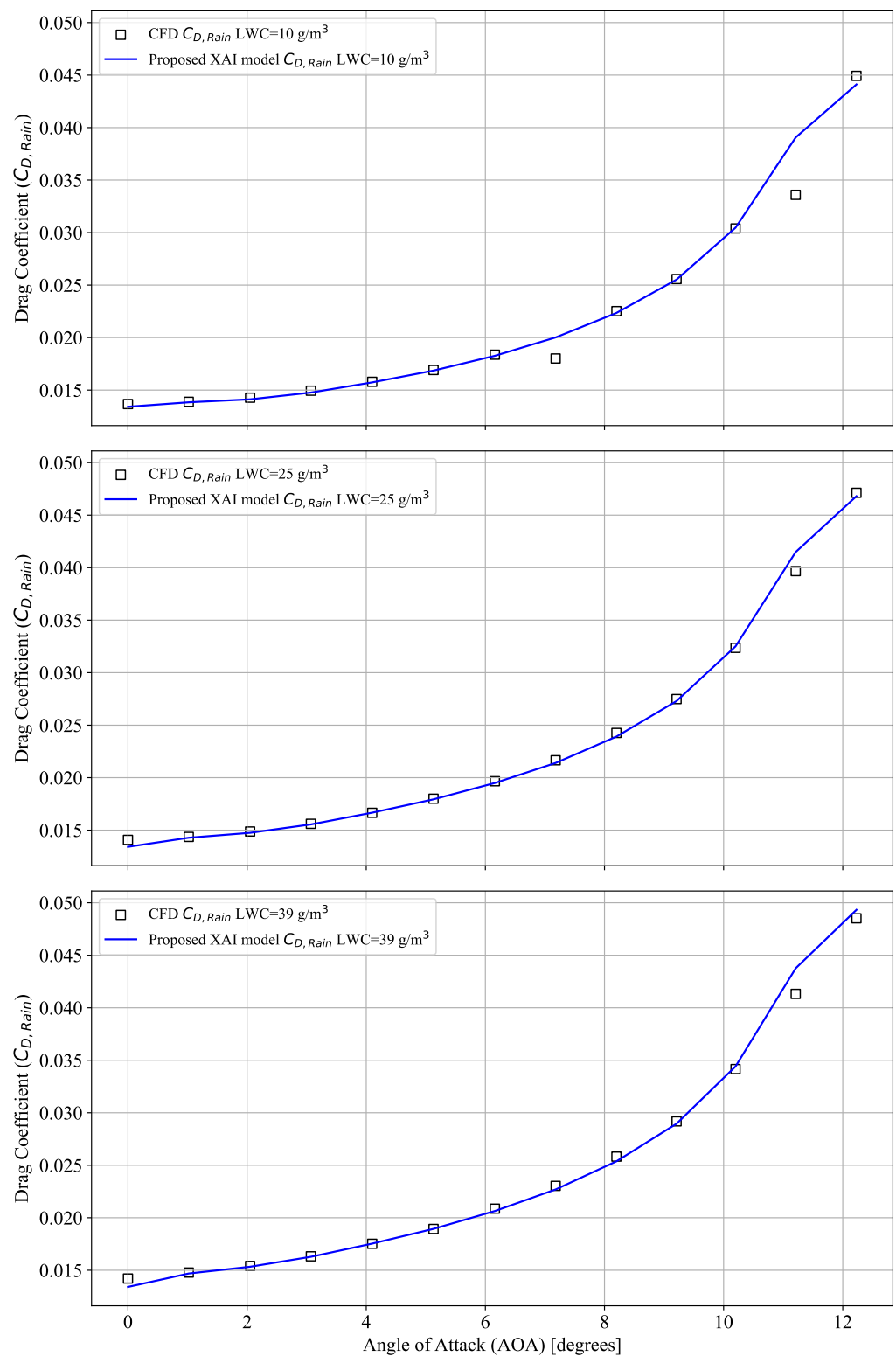


Figure 10. A comparison of the drag coefficient ($C_{D,Rain}$) as a function of the angle of attack (AOA) for different liquid water content (LWC) values. Each subplot represents a different LWC: 10 g/m³, 25 g/m³, and 39 g/m³. The blue line represents the proposed XAI model's $C_{D,Rain}$, while the black hollow squares represent the CFD $C_{D,Rain}$. The model demonstrates a high degree of accuracy with an R^2 value of 0.97.

3.4. BEM Results Using XAI Model

The XAI model developed using symbolic regression was integrated into the Blade Element Momentum (BEM) framework to calculate the aerodynamic forces on the wind turbine blades. These forces were then used to compute the thrust, torque, and, finally, power output under various conditions.

Table 2 presents the wind turbine performance metrics at various wind speeds and LWC levels using the BEM framework. The data reveal how the power output decreases with increasing LWC, indicating the impact of rain conditions on turbine efficiency.

Table 2. Wind turbine performance metrics at various wind speeds and LWC levels using BEM.

Metric	Wind Speed	Dry	LWC 10 g/m ³	LWC 25 g/m ³	LWC 39 g/m ³
Power (kW)	7 m/s	5.92 kW	5.87 kW	5.70 kW	5.58 kW
	10 m/s	11.31 kW	11.10 kW	10.87 kW	10.69 kW
	15 m/s	12.40 kW	12.09 kW	11.88 kW	11.68 kW
	20 m/s	11.29 kW	10.97 kW	10.76 kW	10.56 kW
	25 m/s	10.29 kW	9.98 kW	9.77 kW	9.57 kW

At a wind speed of 7 m/s, the power output decreases from 5.92 kW (dry) to 5.58 kW (LWC 39 g/m³), showing a 5.74% reduction. Similarly, at 10 m/s, the power drops from 11.31 kW (dry) to 10.69 kW (LWC 39 g/m³), representing a 5.48% reduction. At 15 m/s, the power decreases from 12.40 kW (dry) to 11.68 kW (LWC 39 g/m³), indicating a 5.81% reduction. For 20 m/s, the power drops from 11.29 kW (dry) to 10.56 kW (LWC 39 g/m³), showing a 6.46% reduction. Finally, at 25 m/s, the power decreases from 10.29 kW (dry) to 9.57 kW (LWC 39 g/m³), resulting in a 7% reduction.

Figure 11 illustrates the power output versus the wind speed under varying conditions of liquid water content (LWC). The figure further emphasizes the trend of decreasing power output with increasing LWC across different wind speeds, corroborating the data presented in Table 2.

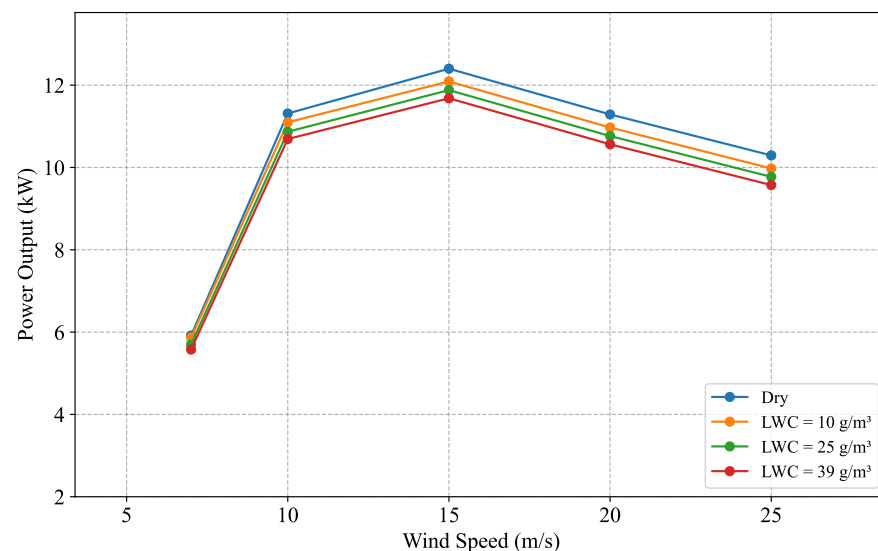


Figure 11. Plot of power output versus wind speed under varying conditions of liquid water content (LWC).

The results demonstrate a consistent decrease in power output with increasing LWC, with the most significant reduction occurring at higher wind speeds. This trend indicates that the impact of rain is more pronounced under these conditions. The degradation in performance can be attributed to the effects of raindrops on the airflow over the turbine blades, which disrupts the smooth flow, increases aerodynamic drag, and reduces overall efficiency.

These findings highlight the importance of considering rain effects in the design and operation of wind turbines to ensure optimal performance under various environmental conditions. The integration of the XAI model within the BEM framework provides a robust tool for predicting and mitigating the adverse impacts of rain on wind turbine performance. Future research could focus on refining these models and exploring mitigation strategies to minimize the impact of rain on wind turbine efficiency.

4. Conclusions and Future Works

This research examined the significant influence of unfavorable weather conditions, particularly rain, on the aerodynamic performance and power generation of horizontal-axis wind turbines (HAWTs) by integrating Blade Element Momentum (BEM) theory with explainable artificial intelligence (XAI). This study offers a comprehensive examination of the S809 airfoil, a commonly used airfoil in wind turbines at the National Renewable Energy Laboratory (NREL), in different rainfall situations.

The research utilized ANSYS FLUENT to perform computational fluid dynamics (CFD) simulations. The simulations employed a two-phase flow model known as the Discrete Phase Model (DPM) to describe rain. The simulations were run at a Reynolds number (Re) of 1×10^6 and liquid water content (LWC) values of 0 (dry), 10, 25, and 39 g/m³. The simulations demonstrated that when exposed to rain, the S809 airfoil experiences a substantial decrease in lift and a rise in drag, resulting in a detrimental impact on its aerodynamic efficiency. The decrease in aerodynamic efficiency was consistent at all angles of attack, demonstrating the harmful impact of rain on the functioning of wind turbines. The decline in lift coefficient ranges from 0.85% to 3.74% for an LWC of 10 g/m³, from 1.91% to 8.20% for an LWC of 25 g/m³, and from 2.98% to 12.70% for an LWC of 39 g/m³. The drag coefficient rises by 1.92% to 6.19% for an LWC of 10 g/m³, 4.94% to 13.90% for an LWC of 25 g/m³, and 5.96% to 21.24% for an LWC of 39 g/m³.

The novel contribution of this research lies in the development of machine learning models using symbolic regression, which predicted changes in aerodynamic coefficients under rainy conditions with high accuracy. These models demonstrated a good prediction with an $R^2 = 0.97$, highlighting their potential to improve the accuracy of wind turbine performance forecasts under challenging weather circumstances using BEM.

The application of the BEM method to estimate the power output of the NREL Phase VI wind turbine under both dry and wet conditions, coupled with machine learning-based correction models, predicted for aerodynamic penalties. The research revealed that rain with an LWC of 10 g/m³ could decrease wind turbine power output within the range of 0.85% to 3.07%. Similarly, rain with an LWC of 25 g/m³ was found to result in a reduction in wind turbine power output ranging from 3.70% to 5.06%. Additionally, rain with an LWC of 39 g/m³ was observed to lead to a decrease in wind turbine power output between 5.74% and 7%. This finding is critical as it quantifies the impact of rain on renewable energy generation, highlighting the need for adaptive strategies and advanced predictive models to mitigate these effects.

In the future, the authors intend to conduct unsteady simulations using a Large Eddy Simulation (LES) of the airfoil and also investigate the effect of rain on the NREL Phase VI wind turbine using a sliding mesh analysis of the full rotor CFD simulation, building upon their previous research [28,62]. Also, the authors intend to take into account different airfoils used in wind turbines to enhance the generalizability of our models.

In summary, this research contributes significantly to the understanding of how environmental conditions, specifically rain, affect the performance of wind turbines. By integrating advanced computational simulations with machine learning techniques, it offers a comprehensive approach to predicting and managing the aerodynamic penalties associated with rain. These insights are essential for improving the reliability and efficiency of wind energy systems, thereby supporting the ongoing transition to sustainable energy solutions. The findings emphasize the importance of considering environmental factors in the design and operation of wind turbines, ensuring optimized performance and maximizing

the potential of renewable energy sources in varying climatic conditions. This investigation not only provides a robust framework for forecasting wind turbine performance in rainy conditions but also showcases the potential of integrating BEM theory with XAI to boost wind farm operational efficiency and safety, heralding future innovations in renewable energy technology and management practices.

Author Contributions: I.F.S.A.K. and M.K.G.—Conceptualization, Data Curation, Formal Analysis, ML-based Symbolic Regression, Visualization, Investigation, Validation, Writing—Original Draft. P.M.P.T.—Simulations, Writing—Original Draft. S.R.B.—Machine Learning and Review. E.Y.-K.N.—Supervision, Writing—Review and Editing. A.M.—Supervision, Writing—Review and Editing. All authors have read and agreed to the published version of the manuscript.

Funding: This research received no external funding.

Institutional Review Board Statement: Not applicable.

Informed Consent Statement: Not applicable.

Data Availability Statement: Access to the data and code used in this study will be made available upon reasonable request. Requests should be directed to Ijaz Fazil Syed Ahmed Kabir at ijaz0001@e.ntu.edu.sg or Mohan Kumar Gajendran at mgz53@umsystem.edu.

Conflicts of Interest: The authors declare no conflicts of interest.

Nomenclature

C_D	Drag Coefficient
C_L	Lift Coefficient
D_p	Diameter of Raindrop (mm)
Re	Reynolds Number
U_T	Terminal Velocity (m/s)

Greek Symbols

α	Angle of Attack (degrees)
----------	---------------------------

Abbreviations

AOA	Angle of Attack
BEM	Blade Element Momentum
CFD	Computational Fluid Dynamics
CSU	Colorado State University
DPM	Discrete Phase Model
DUT	Delft University of Technology
ESCM-WAR	Enhanced Soil Moisture Content Model–Wind And Rain Hybrid Approach
GWEC	Global Wind Energy Council
HAWT	Horizontal-Axis Wind Turbine
IEA	International Energy Agency
LWC	Liquid Water Content
MOCO	Multi-objective Combinatorial Optimization
MRF	Multiple Reference Frame
NREL	National Renewable Energy Laboratory
OSU	Ohio State University
RANS	Reynolds-Averaged Navier–Stokes
Re	Reynolds Number
SST	Shear Stress Transport
VAWT	Vertical-Axis Wind Turbine
VOF	Volume of Fluid
XAI	Explainable Artificial Intelligence

References

1. Van de Graaf, T.; Lesage, D. The International Energy Agency after 35 years: Reform needs and institutional adaptability. *Rev. Int. Organ.* **2009**, *4*, 293–317. [[CrossRef](#)]
2. Global Wind Energy Council. *GWEC Global Wind Report 2019*; Global Wind Energy Council: Bonn, Germany, 2017.

3. Nazir, M.S.; Ali, N.; Bilal, M.; Iqbal, H.M. Potential environmental impacts of wind energy development: A global perspective. *Curr. Opin. Environ. Sci. Health* **2020**, *13*, 85–90. [CrossRef]
4. Wu, Z.; Cao, Y.; Nie, S.; Yang, Y. Effects of rain on vertical axis wind turbine performance. *J. Wind. Eng. Ind. Aerodyn.* **2017**, *170*, 128–140. [CrossRef]
5. Ke, S.; Yu, W.; Wang, T.; Ge, Y. Aerodynamic performance and wind-induced effect of large-scale wind turbine system under yaw and wind-rain combination action. *Renew. Energy* **2019**, *136*, 235–253. [CrossRef]
6. Corrigan, R.D.; DeMiglio, R.D. Effect of Precipitation on Wind Turbine Performance. Technical Report. 1985. Available online: <https://ntrs.nasa.gov/citations/19850019074> (accessed on 18 July 2024).
7. Shankar Verma, A.; Jiang, Z.; Ren, Z.; Hu, W.; Teuwen, J.J. Effects of onshore and offshore environmental parameters on the leading edge erosion of wind turbine blades: A comparative study. *J. Offshore Mech. Arct. Eng.* **2021**, *143*, 042001. [CrossRef]
8. Rhode, R.V. *Some Effects of Rainfall on Flight of Airplanes and on Instrument Indications*; Technical Report; National Advisory Committee for Aeronautics: Washington, DC, USA, 1941.
9. Hansman, R.J., Jr.; Barsotti, M.F. Surface wetting effects on a laminar flow airfoil in simulated heavy rain. *J. Aircr.* **1985**, *22*, 1049–1053. [CrossRef]
10. Hansman, R.J., Jr.; Craig, A.P. Low Reynolds number tests of NACA 64-210, NACA 0012, and Wortmann FX67-K170 airfoils in rain. *J. Aircr.* **1987**, *24*, 559–566. [CrossRef]
11. Marchman, J., III; Robertson, E.A.; Emsley, H.T. Rain effects at low Reynolds number. *J. Aircr.* **1987**, *24*, 638–644. [CrossRef]
12. Bezos, G.M.; Dunham, R.E., Jr.; Gentry, G.L., Jr.; Melson, W.E., Jr. *Wind Tunnel Aerodynamic Characteristics of a Transport-Type Airfoil in a Simulated Heavy Rain Environment*; Technical Report; NASA Langley Research Center: Hampton, VA, USA, 1992.
13. Valentine, J.R.; Decker, R.A. Tracking of raindrops in flow over an airfoil. *J. Aircr.* **1995**, *32*, 100–105. [CrossRef]
14. Thompson, B.E.; Marrochello, M.R. Rivulet formation in surface-water flow on an airfoil in rain. *AIAA J.* **1999**, *37*, 45–49. [CrossRef]
15. Tan, J.; Papadakis, M.; Sampath, M. *Computational Study of Large Droplet Breakup in the Vicinity of an Airfoil*; US Department of Transportation, Federal Aviation Administration, Office of Aviation Research: Washington, DC, USA, 2005.
16. Wan, T.; Wu, S.W. Aerodynamic analysis under influence of heavy rain. In Proceedings of the 24th International Congress of the Aeronautical Sciences, Yokohama, Japan, 29 August–3 September 2004.
17. Zhang, R.-m.; Cao, Y.-h. Study of aerodynamic characteristics of an airfoil in rain. *J. Aerosp. Power* **2010**, *25*, 2064–2069.
18. Douvi, E.C.; Margaritis, D.P. Aerodynamic performance investigation under the influence of heavy rain of a NACA 0012 airfoil for wind turbine applications. *Int. Rev. Mech. Eng.* **2012**, *6*, 1228–1235. [CrossRef]
19. Cai, M.; Abbasi, E.; Arastoopour, H. Analysis of the Performance of a Wind-Turbine Airfoil under Heavy-Rain Conditions Using a Multiphase Computational Fluid Dynamics Approach. *Ind. Eng. Chem. Res.* **2013**, *52*, 3266–3275. [CrossRef]
20. Douvi, E.C.; Margaritis, D.P.; Lazaropoulos, S.D.; Svanas, S. Low Reynolds number investigation of the flow over a NACA 0012 airfoil at different rainfall rates. *Int. Rev. Mech. Eng.* **2013**, *7*, 625–632. [CrossRef]
21. Douvi, E.C.; Margaritis, D.P.; Lazaropoulos, S.D.; Svanas, S.G. Experimental and computational study of the effects of different liquid water content on the aerodynamic performance of a NACA 0012 airfoil at low Reynolds number. In Proceedings of the 5th International Conference on Experiments/Process/System Modeling/Simulation/Optimization, Athens, Greece, 3–6 July 2013; Athens Institute for Education and Research: Athens, Greece, 2013; p. 9.
22. Cohan, A.C.; Arastoopour, H. Numerical simulation and analysis of the effect of rain and surface property on wind-turbine airfoil performance. *Int. J. Multiph. Flow* **2016**, *81*, 46–53. [CrossRef]
23. Douvi, E.; Douvi, D.; Pylarinos, D.; Margaritis, D. Effect of Rain on the Aerodynamic Performance of a Horizontal Axis Wind Turbine—A Computational Study. *Int. J. Energetica (IJECA)* **2021**, *6*, 35–43.
24. Gahlot, A.; Sankar, L.; Pichitkul, A. Computational Modeling of the Effects of Rain on Wind Turbine Performance. In Proceedings of the Turbo Expo: Power for Land, Sea, and Air. American Society of Mechanical Engineers (ASME), Rotterdam, The Netherlands, 13–17 June 2022; Volume 86137, p. V011T38A016.
25. Wu, S.; Sun, H.; Zheng, X. A numerical study on dynamic characteristics of 5 MW floating wind turbine under wind-rain conditions. *Ocean Eng.* **2022**, *262*, 112095. [CrossRef]
26. Hu, H.; Sista, H.; Dhulipalla, A.; Kurmar, A.; Hu, H. An Experimental Study on the Detrimental Effects of Rainfall on the Aerodynamic Performance of a Wind Turbine Blade Model. *Bull. Am. Phys. Soc.* **2023**. Available online: <https://meetings.aps.org/Meeting/DFD23/Session/T04.8> (accessed on 18 July 2024).
27. Letzgus, S.; Müller, K.R. An explainable AI framework for robust and transparent data-driven wind turbine power curve models. *Energy AI* **2024**, *15*, 100328. [CrossRef]
28. Kabir, I.F.S.A.; Ng, E. Insight into stall delay and computation of 3D sectional aerofoil characteristics of NREL phase VI wind turbine using inverse BEM and improvement in BEM analysis accounting for stall delay effect. *Energy* **2017**, *120*, 518–536. [CrossRef]
29. Kabir, I.F.S.A. Improvement of BEM Analysis to Incorporate Stall Delay Effect and the Study of Atmospheric Boundary Layer Effect on the Wake Characteristics of NREL Phase VI Turbine. Ph.D. Thesis, Nanyang Technological University, Singapore, 2018. Available online: <https://hdl.handle.net/10356/75824> (accessed on 18 July 2024).
30. Cao, Y.; Wu, Z.; Xu, Z. Effects of rainfall on aircraft aerodynamics. *Prog. Aerosp. Sci.* **2014**, *71*, 85–127. [CrossRef]

31. Valentine, J.; Decker, R. A Lagrangian-Eulerian scheme for flow around an airfoil in rain. *Int. J. Multiph. Flow* **1995**, *21*, 639–648. [CrossRef]
32. Wu, Z.; Cao, Y.; Ismail, M. Numerical simulation of airfoil aerodynamic penalties and mechanisms in heavy rain. *Int. J. Aerosp. Eng.* **2013**, *2013*, 590924. [CrossRef]
33. Douvi, E.; Margaris, D. Simulation of heavy rain flow over a NACA 0012 airfoil. In Proceedings of the 4th International Conference on Experiments/Process/System Modeling/Simulation/Optimization (4th IC-EpsMsO), Athens, Greece, 6–9 July 2011.
34. Ismail, M.; Cao, Y.H. Airfoils Aerodynamic Performance Analysis in Heavy Rain. *Appl. Mech. Mater.* **2013**, *245*, 297–302. [CrossRef]
35. Wan, T.; Pan, S.P. Aerodynamic efficiency study under the influence of heavy rain via two-phase flow approach. In Proceedings of the 27th International Congress of the Aeronautical Sciences, Nice, France, 19–24 September 2010; Volume 2, pp. 1343–1353.
36. Ismail, M.; Yihua, C.; Bakar, A.; Wu, Z. Aerodynamic efficiency study of 2D airfoils and 3D rectangular wing in heavy rain via two-phase flow approach. *Proc. Inst. Mech. Eng. Part G J. Aerosp. Eng.* **2014**, *228*, 1141–1155. [CrossRef]
37. Fatahian, H.; Salarian, H.; Eshagh Nimvari, M.; Khaleghinia, J. Numerical simulation of the effect of rain on aerodynamic performance and aeroacoustic mechanism of an airfoil via a two-phase flow approach. *SN Appl. Sci.* **2020**, *2*, 867. [CrossRef]
38. Shapiro, A. Drag-induced transfer of horizontal momentum between air and raindrops. *J. Atmos. Sci.* **2005**, *62*, 2205–2219. [CrossRef]
39. Markowitz, A.H. Raindrop size distribution expressions. *J. Appl. Meteorol. (1962–1982)* **1976**, *15*, 1029–1031. [CrossRef]
40. Ansys Fluent. *Ansys Fluent Theory Guide*; Ansys Inc.: Canonsburg, PA, USA, 2021.
41. Satheesh, C.; Parthasarathy, G. Analysis of Airfoil Aerodynamic Performance in Heavy Rain. *Int. J. Nov. Res. Eng. Sci.* **2015**, *2*, 41–49. Available online: www.noveltyjournals.com (accessed on 18 July 2024).
42. Fatahian, H.; Salarian, H.; Nimvari, M.E.; Khaleghinia, J. Computational fluid dynamics simulation of aerodynamic performance and flow separation by single element and slatted airfoils under rainfall conditions. *Appl. Math. Model.* **2020**, *83*, 683–702. [CrossRef]
43. Patel, P.Y.; Liu, J.H.; Vantsevich, V.V.; Koomullil, R.P. Modelling effect of rain on aerodynamic performance of the Ahmed body. In Proceedings of the AIAA SCITECH 2022 Forum, Reston, VA, USA, 3–7 January 2022; p. 0335.
44. Jonkman, J.M. *Modeling of the UAE Wind Turbine for Refinement of FAST_AD*; Technical Report; National Renewable Energy Lab. (NREL): Golden, CO, USA, 2003.
45. Morales, C.O.; Vázquez, K.R. Symbolic regression problems by genetic programming with multi-branches. In *Proceedings of the Mexican International Conference on Artificial Intelligence*; Springer: Berlin/Heidelberg, Germany, 2004; pp. 717–726.
46. Stinstra, E.; Rennen, G.; Teeuwen, G. Metamodeling by symbolic regression and Pareto simulated annealing. *Struct. Multidiscip. Optim.* **2008**, *35*, 315–326. [CrossRef]
47. Kirkpatrick, S.; Gelatt, C.D.; Vecchi, M.P. Optimization by simulated annealing. *Science* **1983**, *220*, 671–680. [CrossRef] [PubMed]
48. Gajendran, M.K.; Kabir, I.F.S.A.; Vadivelu, S.; Ng, E.Y.K. Machine Learning-Based Approach to Wind Turbine Wake Prediction under Yawed Conditions. *J. Mar. Sci. Eng.* **2023**, *11*, 2111. [CrossRef]
49. Burton, T.; Sharpe, D.; Jenkins, N.; Bossanyi, E. *Wind Energy Handbook*; John Wiley & Sons, Ltd: Chichester, UK; New York, NY, USA; Weinheim, Germany; Brisbane, Australia; Singapore; Toronto, ON, Canada, 2001.
50. Hansen, M.O.L. *Aerodynamics of Wind Turbines*, 2nd ed.; Earthscan: London, UK; Sterling, VA, USA, 2008.
51. Marten, D.; Wendler, J. QBlade Short Manual. 2018. Available online: <https://api-depositonce.tu-berlin.de/server/api/core/bitstreams/18070cae-11b3-4ae0-a9d0-b97b41f427b6/content> (accessed on 18 July 2024).
52. Moriarty, P.J.; Hansen, A.C. *AeroDyn Theory Manual*; Technical Report NREL/TP-500-36881; National Renewable Energy Laboratory: Golden, CO, USA, 2005; Prepared under Task No. WER4.3101 and WER5.3101.
53. Larsen, T.J.; Hansen, A.M. *How 2 HAWC2, the User's Manual*, version 12.7 ed.; Edited by the DTU Wind Energy HAWC2 Development Team; Risø National Laboratory: Roskilde, Denmark, 2019. ISBN 978-87-550-3583-6. ISSN 0106-2840;
54. Platt, A.D.; Buhl, M.L., Jr. *WT_Perf User Guide for Version 3.05.00*; Technical Report NREL/TP-500-36881; National Renewable Energy Laboratory: Golden, CO, USA, 2012; Revised November 9, 2012 for WT_Perf v3.05.00a-adp.
55. Jonkman, J.M.; Buhl, M.L., Jr. *FAST User's Guide*; Technical Report NREL/TP-500-38230; National Renewable Energy Laboratory: Golden, CO, USA, 2005; Updated August 2005. Prepared under Task Nos. WER1.1220, WER2.1220, WER3.1910, WER4.3102, and WER5.3115. Available online: <https://www.nrel.gov/docs/fy06osti/38230.pdf> (accessed on 31 July 2024).
56. Bossanyi, E.A.; Quarton, D.C. *GH Bladed Theory Manual*; Garrad Hassan and Partners Limited: Bristol, UK, 2003; Commercial in Confidence.
57. Lindenburg, C. *PHATAS Release “NOV-2003” and “APR-2005” User's Manual*; Technical Report ECN-I-05-005; Energy Research Centre of the Netherlands (ECN): Petten, The Netherlands, 2005.
58. Syed Ahmed Kabir, I.F.; Gajendran, M.K.; Ng, E.Y.K.; Mehdizadeh, A.; Berrouk, A.S. Novel Machine-Learning-Based Stall Delay Correction Model for Improving Blade Element Momentum Analysis in Wind Turbine Performance Prediction. *Wind* **2022**, *2*, 636–658. [CrossRef]
59. Martinez, J.; Flaszynski, P.; Doerffer, P.; Szulc, O. Improvement of wind turbine blade performance by means of rod vortex generators. In *MARE-WINT: New Materials and Reliability in Offshore Wind Turbine Technology*; Springer International Publishing: Cham, Switzerland, 2016; pp. 81–102.

60. Zhong, J.; Li, J.; Guo, P. Effects of leading-edge rod on dynamic stall performance of a wind turbine airfoil. *Proc. Inst. Mech. Eng. Part A J. Power Energy* **2017**, *231*, 753–769. [[CrossRef](#)]
61. Douvi, D.C.; Margaris, D.P.; Davaris, A.E. Aerodynamic performance of a NREL S809 airfoil in an air-sand particle two-phase flow. *Computation* **2017**, *5*, 13. [[CrossRef](#)]
62. Syed Ahmed Kabir, I.F.; Ng, E. Effect of different atmospheric boundary layers on the wake characteristics of NREL phase VI wind turbine. *Renew. Energy* **2019**, *130*, 1185–1197. [[CrossRef](#)]

Disclaimer/Publisher’s Note: The statements, opinions and data contained in all publications are solely those of the individual author(s) and contributor(s) and not of MDPI and/or the editor(s). MDPI and/or the editor(s) disclaim responsibility for any injury to people or property resulting from any ideas, methods, instructions or products referred to in the content.